Novel Signal Detectors for Ambient Backscatter Communications in Internet of Things Applications

Yunfei Chen, *Senior Member, IEEE*, and Wei Feng, *Senior Member, IEEE*

***Abstract*—Ambient backscatter communication (AmBC) enables low-cost low-rate wireless interconnections for Internet of Things (IoT) applications. In this work, new signal detectors for different cases of AmBCs are derived. Specifically, both coherent and partially coherent detectors are obtained for the Gaussian ambient signals and phase shift keying (PSK) ambient signals. The maximum likelihood (ML) detection method and improved energy detection method (including energy detection and magnitude detection as special cases) are adopted. Numerical results show that the energy detection method has the best performance when the ambient signals are Gaussian, while the magnitude detection method has the best performance when the ambient signals are PSK modulated. Both are comparable to the optimum ML detection. Numerical results also show that the improved energy detection method is very flexible and that detectors for PSK ambient signals are slightly better than those for the Gaussian ambient signals.**

***Index Terms*—Ambient backscatter communications (AmBCs), maximum likelihood (ML), signal detection.**

I. Introduction

BACKSCATTER communication has been widely used in radio-frequency identification (RFID) systems, where the tag reader sends a radio frequency (RF) signal to a remote tag and the remote tag responds by modulating and reflecting the received signal to deliver the information [1]. To further reduce the cost of the system, ambient backscatter communication (AmBC) has also been proposed, where the remote tag reflects an ambient RF signal instead of a dedicated signal from the tag reader [2]. The AmBC systems provide a useful enabling technology for Internet of Things (IoT), because most IoT applications are restricted by energy and cost for a large-scale deployment, while AmBC has low-cost and low-energy consumption to become a perfect match with IoT. For example, in logistics and warehouse management, the tags attached to inventories can use AmBC to send information to the reader for tracking [2]. In smart homes, the WiFi router can collect sensing information from tags located indoor for automatic adjustment of temperature and lights etc. [3]. In healthcare, AmBC can be used in implants where WiFi signals act as RF sources [4]. In environmental monitoring, AmBC tags can be used to monitor humidity, water quality, and poisonous gas to detect anomalies [5]. Due to its importance, a lot of works have been conducted to build efficient AmBC systems, including [4], [6], [7], [8], and [9]. For example, in [10], the ambient pilot symbols used in existing systems for orthogonal frequency-division multiplexing (OFDM) were applied in backscatter communication. Two modulation schemes and an optimal maximum likelihood (ML) detector were proposed. In [11], the capacity of legacy and backscatter channels were analyzed for different receivers and it was shown that the interference from backscatter can be turned into a form of multipath diversity for the legacy system, while the backscatter system can achieve satisfactory date rates over short distances. In [12], a cloud radio access network was considered where the performance of the secondary backscatter node was evaluated considering training-based channel estimation, practical modulation constraints, and imperfect direct-link interference suppression. Based on this, its transmission rate was optimized. In [13], spatial modulation and spatial multiple access were applied to AmBC. A modified ML detector and multiuser sparse Bayesian learning-based detector were proposed to detect the backscattered signal. A comprehensive survey on different aspects of AmBC is provided in [14].

In the design of an efficient AmBC system, the signal detector is a key component. Hence, much research effort has been spent on signal detector designs for AmBC. To name a few, in [15], [16], and [17], assuming Gaussian ambient signals, differential encoding was applied to the transmitted signal and then a Gaussian approximation was used to derive the ML detectors. In [18] and [19], both coherent detectors and energy detectors were proposed for AmBC, where the ambient RF signal is assumed to be either a Gaussian or phase-shift keying (PSK) modulated. In [20], the tag signal was first encoded using the Manchester coding, and then the corresponding ML detector was proposed for both the Gaussian and PSK ambient signals. Qian et al. [21] proposed ML and energy detectors for noncoherent detection, where the ambient signal was also assumed a Gaussian and differential encoding was used, similar to [15], [16], and [17]. In [22], ternary coded signals were used, where the tag has three states, and a maximum a posteriori detector was proposed to detect these signals, again for

Manuscript received 2 June 2022; revised 14 February 2023 and 6 July 2023; accepted 11 August 2023. Date of publication 16 August 2023; date of current version 24 January 2024. The work of Wei Feng was supported in part by the National Natural Science Foundation of China under Grant 62341110 and Grant U22A2002; in part by the National Key Research and Development Program of China under Grant 2020YFA0711301; and in part by the Suzhou Science and Technology Project. The work of Yunfei Chen was supported in part by the King Abdullah University of Science and Technology Research Funding (KRF) under Award ORA-2021-CRG10-4696. *(Corresponding author: Wei Feng.)*

Yunfei Chen is with the Department of Engineering, University of Durham, DH1 3LE Durham, U.K. (e-mail: Yunfei.Chen@durham.ac.uk).

Wei Feng is with the Beijing National Research Center for Information Science and Technology, Department of Electronic Engineering, Tsinghua University, Beijing 100084, China (e-mail: fengwei@tsinghua.edu.cn).

Digital Object Identifier 10.1109/JIOT.2023.3305645

the Gaussian ambient sources. Zhang et al. [23] proposed a constellation learning-based detection by inserting two known labels into the data frame. In [24], a new covariance-based detector was proposed for AmBC, while in [25], the optimal noncoherent detector for AmBC that does not require any channel knowledge was proposed and analyzed. More works on noncoherent detection can be found in [26], [27], [28], [29], [30], [31], and [32]. Devineni and Dhillon [26], [27], [28] derived a new receiver for a first-order autoregressive channel and its bit error rate (BER) was analyzed. Devineni and Dhillon [29] analyzed the performance of a Manchester encoded symbol detection and showed its performance gain over the on-off keying (OOK). Yang et al. [30] used a modified expectation maximization method to cluster signals from multiple tags and then a mapping between the clusters and the transmitted symbols to recover signals without channel state information. Qian et al. [31] extended a binary modulation to an M-ary modulation, while Duan et al. [32] proposed a sample covariance matrix distance-based rule to detect backscatter symbols using time correlation in OFDM. In [33] and [34], the performances of AmBC in terms of capacity, outage, and BER were analyzed for ML and energy detectors using a Gaussian approximation when the ambient signal is PSK modulated. Yang et al. [35], Darsena [36], and ElMossallamy et al. [37] studied the energy detection for AmBC systems using OFDM signals by taking advantage of the special structure of multicarrier systems. Kang et al. [38], Tao et al. [39], Liu et al. [40], and Chen et al. [41] investigated signal detection for AmBC systems using multiple antennas. In [42], the optimal detector for OOK was proposed and an energy detector was used as a benchmark, for multiantenna systems. Yang et al. [43] also studied a multiantenna AmBC system but the tag was used as a passive relay to help the detection of the signal from the RF source instead of the signal from the tag.

All the aforementioned works have provided very useful guidance on the designs of AmBC systems. However, there are several important issues that require further investigation.

1) Most existing detectors have assumed the Gaussian ambient signals. Qian et al. [18] and Tao et al. [20] assumed PSK ambient signals but they used the energy detector directly without deriving the optimal detector. Thus, it is of great interest to derive new detectors for PSK ambient signals.
2) The detectors in [15], [16], [17], [18], [19], [20], [21], [22], [23], and [24] require the channel state information of all three links in AmBC, while the detectors in [25] does not require any channel state information. In practice, channel state information may be available in some links but not available in other links. For example, the channel between the ambient RF source and the reader may be estimated at the reader blindly or by using pilots, while this might be difficult for the channel between the ambient RF source and the tag or the channel between the tag and the reader due to the limited processing capability at the tag. Thus, in addition to the case when all channel state information is available, it is useful to derive new detectors for the case when only partial information is available for partially coherent detection.
3) The energy detector is widely used in AmBC. On the other hand, it is well known that the improved energy detector (IED) could outperform the conventional energy detector by replacing the squaring operation in the energy detection with an arbitrary powering operation [44]. Moreover, the IED includes the energy and magnitude detectors as special cases. Most existing works studied the conventional energy detector but not the IED or the magnitude detector. It is of great interest to examine how these detectors perform in AmBC.

Motivated by the above observations, in this work, new signal detectors for AmBC will be derived. Specifically, four different cases will be considered: 1) coherent detection assuming the Gaussian ambient signals; 2) coherent detection assuming PSK ambient signals; 3) partial coherent detection assuming the Gaussian ambient signals; and 4) partial coherent detection assuming PSK ambient signals. For coherent detection, channel state information of all links is required, while for partial coherent detection, only channel state information of the source-to-reader (SR) link is required, at the receiver. For each case, new detectors will be obtained, including ML, IED, energy, and magnitude detectors.

Numerical results show that the energy detector performs the best when the ambient signal is Gaussian, while the magnitude detector performs the best when the ambient signal is PSK modulated, both of which are almost as good as the corresponding ML detectors but with much lower complexity. Numerical results also show that the IED is very general and that the change of its performance with the power value depends on the case considered. Moreover, detectors assuming PSK ambient signals are slightly better than those assuming the Gaussian ambient signals. The novelty and the contribution of this work can be summarized as follows.

1) Compared with existing works on coherent detection, including [18] and [20], our IED and magnitude detectors are new. Also, our ML and energy detectors for PSK ambient signals are new. They have never been derived before. In the derivation, the Gaussian approximation method is used, similar to that in [18] and [20], but this is a very general method that has been widely used in many wireless techniques. These will be presented in Sections III-A and III-B.
2) Compared with existing works on noncoherent detection, including [25], our IED detectors are new. Also, the case with PSK ambient signals has not been studied in [25]. The ML method for the Gaussian signals is similar to that in [25] but assuming different channel knowledge leads to totally different detectors. These will be presented in Sections III-C and III-D.
3) The ML method is used. When this becomes too challenging, the moment-matching approximation is used. The new detectors outperform the existing detectors in most cases. They provide a comprehensive study of signal detection for AmBC systems.

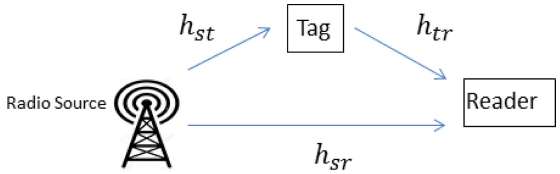

Fig. 1. System model considered.

II. System Model

Consider a single-carrier and single-antenna AmBC system, similar to those in [15], [16], [17], [18], [19], [20], [21], [22], [23], and [24]. In this system, there are three links: 1) the source-to-tag (ST) link; 2) the tag-to-reader (TR) link; and 3) the SR link. The source radiates an ambient RF signal $s[n]$, where $n = 1, 2, \ldots, N$ index the samples. This signal arrives at the reader via the SR link and at the tag via the ST link. When the tag wants to send a bit "0" to the reader, it will not reflect the received source signal. When the tag wants to send a bit "1" to the reader, it adjusts its impedance to reflect the received source signal so that the reader will receive the reflected signal via the TR link, in addition to the direct signal received from the SR link. The system model is shown in Fig. 1. Practical applications of this system include IoT sensors for environment monitoring and RF identification (RFID) tags for inventory checking and localization. Table I lists the notations frequently used in the derivation later.

Thus, the received signal at the reader when bit "0" is sent by the tag can be given by

$$y[n] = h_{sr}s[n] + w[n] \tag{1}$$

and the received signal at the reader when bit "1" is sent by the tag can be given by

$$y[n] = h_{sr}s[n] + \eta h_{tr}h_{st}s[n] + w[n] \tag{2}$$

where h_{sr} is the channel coefficient of the SR link, h_{tr} is the channel coefficient of the TR link, h_{st} is the channel coefficient of the ST link, η is the constant reflection coefficient at the tag, and $w[n]$ is the additive white Gaussian noise (AWGN) with $w[n] \sim \mathcal{CN}(0, \sigma_w^2)$. In the Rayleigh fading channels, h_{sr}, h_{tr}, and h_{st} are the complex Gaussian random variables with means zero and variances σ_{sr}^2, σ_{tr}^2, and σ_{st}^2, respectively. The values of σ_{sr}^2, σ_{tr}^2, and σ_{st}^2 are determined by the path loss in the links, which are assumed to follow a free-space path loss model in this work. However, the results can be applied to any path loss models, as the detectors only require values of σ_{sr}^2, σ_{tr}^2, and σ_{st}^2, not the distances that determine the variances. In (1) and (2), $h_{sr}s[n]$ is the direct signal from the ambient source, while $\eta h_{tr}h_{st}s[n]$ is the reflected signal from the ambient source via the tag. These two equations can be combined as

$$y[n] = h_{sr}s[n] + \eta h_{tr}h_{st}s[n]d + w[n] \tag{3}$$

where d is the data bit transmitted by the tag with $d = 0$ for bit "0" and $d = 1$ for bit "1." The tag has a much lower data rate than the ambient source so it is reasonable to assume that d does not change within N samples of the source signal. The above assumes OOK for the remote tag. Other modulation schemes, such as PSK, may also be used for the tag to improve performance. However, the AmBC system and its signal detection will become more complicated [45]. In most RFID applications, simplicity is more important than performance to reduce the deployment cost and thus, only OOK will be considered in the following.

Using $y[n]$, $n = 1, 2, \ldots, N$, the signal detector at the tag reader needs to determine whether $d = 0$ or $d = 1$. For later use, define the hypothesis that $d = 0$ as H_0, the hypothesis

TABLE I
List of Frequently Used Notations

Symbol	Definition
H_0	Hypothesis for bit '0'
H_1	Hypothesis for bit '1'
N	Number of samples
$s[n]$	The n-th sample of ambient RF signal
$y[n]$	The n-th sample of received signal
h_{sr}	Channel coefficient of the SR link
h_{tr}	Channel coefficient of the TR link
h_{st}	Channel coefficient of the ST link
η	Reflection coefficient at the tag
$w[n]$	The n-th sample of noise
σ_{sr}^2	Variance of h_{sr}
σ_{tr}^2	Variance of h_{tr}
σ_{st}^2	Variance of h_{st}
σ_w^2	Variance of noise $w[n]$
h_0	Effective channel coefficient for bit '0'
h_1	Effective channel coefficient for bit '1'
P_s	Variance of ambient signal $s[n]$
p	Order of IED
P_e	Bit error rate
$\Gamma(\cdot)$	the Gamma function
$G(\cdot)$	Gaussian Q function
$I_0(\cdot)$	zero-th order modified Bessel function of the first type
$I_{N-1}(\cdot)$	(N-1)-th order modified Bessel function of the first type
$L(\cdot)$	the Laguerre polynomial
$K_{2p}(\cdot)$	2p-th order modified Bessel function of the second type
$Q_N(\cdot,\cdot)$	N-th order generalized Marcum Q function
U_1	Decision variable of IED in case 1
μ_{10}	Mean of U_1 in H_0
σ_{10}^2	Variance of U_1 in H_0
μ_{11}	Mean of U_1 in H_1
σ_{11}^2	Variance of U_1 in H_1
T_{1IED}	Detection threshold of IED in case 1
Z_1	Decision variable of ED in case 1
R_1	Decision variable of MD in case 1
T_{1MDNak}	Detection threshold of MD in case 1
T_{2ML}	Detection threshold of ML in case 2
U_2	Decision variable of IED in case 2
μ_{20}	Mean of U_2 in H_0
σ_{20}^2	Variance of U_2 in H_0
μ_{21}	Mean of U_2 in H_1
σ_{21}^2	Variance of U_2 in H_1
T_{2IED}	Detection threshold of IED in case 2
Z_2	Decision variable of ED in case 2
R_2	Decision variable of MD in case 2
T_{2ED}	Detection threshold of ED in case 2
U_3	Decision variable of IED in case 3
μ_{30}	Mean of U_3 in H_0
σ_{30}^2	Variance of U_3 in H_0
μ_{31}	Mean of U_3 in H_1
σ_{31}^2	Variance of U_3 in H_1
T_{3IED}	Detection threshold of IED in case 3
U_4	Decision variable of IED in case 4
μ_{40}	Mean of U_4 in H_0
σ_{40}^2	Variance of U_4 in H_0
μ_{41}	Mean of U_4 in H_1
σ_{41}^2	Variance of U_4 in H_1
T_{4IED}	Detection threshold of IED in case 4

that $d = 1$ as H_1, $h_0 = h_{sr}$, and $h_1 = h_{sr} + \eta h_{tr} h_{st}$. Note that this model applies to static AWGN channels or slow fading channels when h_0 and h_1 do not change during the signal detection. In the case of slow fading, the fading coefficients will be decided in the same way as static AWGN channels. For fast-fading channels, the results in this article will not be applicable. Note also that this work assumes frequency-flat fading, binary modulation at the tag, and a single tag scenario, as shown in (3). These assumptions may be different from or more restrictive than those in [10], [11], [12], and [13] but they follow the same model as that in [15], [16], [17], [18], [19], [20], [21], [22], [23], and [24], since the purpose of this work is to extend the energy detectors derived in [18] and [20] to the new optimal detectors and the detectors in [15], [16], [17], [18], [19], [20], [21], [22], [23], and [24] to partially coherent detectors under similar scenarios. One may extend our new detectors further to an M-ary modulation by using the method in [31], to multiple tags by using the method in [30], and to frequency-selective fading channels by using OFDM and the method in [46]. These extensions will not be covered here but could be future works. Next, the new detectors will be derived.

III. Derivation of New Detectors

A. Coherent Detection for Gaussian Signals

We start with the case when all of h_{sr}, h_{tr}, and h_{st} or both h_0 and h_1 are known, and the ambient signal is a Gaussian distributed with $s[n] \sim \mathcal{CN}(0, P_s)$. This case has been studied in [18] and [20] for ML detection. The novelty here is the newly derived IED and magnitude detectors using the same channel knowledge.

1) ML Detector: The ML detector in this case has been derived as [18, eq. (8)], and its BER was also derived in [18, eqs. (13) and (15)]. To avoid confusion, these equations are not listed here and interested readers can refer to [18].

2) IED: Next, we will derive the new IED, which includes the energy detector and the magnitude detector as special cases. Define $U_1 = \sum_{n=1}^{N} |y[n]|^p$ in this case, where p is an arbitrary real number. When $p = 1$, it gives the magnitude detector, and when $p = 2$, it gives the energy detector.

In this case, since $|y[n]|$ is a Rayleigh distributed, U_1 is a sum of independent generalized Gamma random variables. Its PDF does not have a closed-form expression. Thus, approximations have to be used. We will use moment-matching. Using [47, eq. (1-2-130)], the mean and variance of U_1 can be derived as

$$\mathrm{E}\{U_1|H_0\} = N\Gamma\left(1+\frac{p}{2}\right)\left(|h_0|^2 P_s + \sigma_w^2\right)^{\frac{p}{2}} \tag{4a}$$

$$\mathrm{Var}\{U_1|H_0\} = N\left[\Gamma(1+p) - \Gamma^2\left(1+\frac{p}{2}\right)\right]\left(|h_0|^2 P_s + \sigma_w^2\right)^{p} \tag{4b}$$

$$\mathrm{E}\{U_1|H_1\} = N\Gamma\left(1+\frac{p}{2}\right)\left(|h_1|^2 P_s + \sigma_w^2\right)^{\frac{p}{2}} \tag{4c}$$

$$\mathrm{Var}\{U_1|H_1\} = N\left[\Gamma(1+p) - \Gamma^2\left(1+\frac{p}{2}\right)\right]\left(|h_1|^2 P_s + \sigma_w^2\right)^{p} \tag{4d}$$

where $\Gamma(\cdot)$ is the Gamma function [48, eq. (8.310.1)].

Thus, if the Gaussian approximation is used, one has

$$f(U_1|H_0) \approx \frac{1}{\sqrt{2\pi\sigma_{10}^2}} e^{-\frac{(U_1-\mu_{10})^2}{2\sigma_{10}^2}} \tag{5}$$

and

$$f(U_1|H_1) \approx \frac{1}{\sqrt{2\pi\sigma_{11}^2}} e^{-\frac{(U_1-\mu_{11})^2}{2\sigma_{11}^2}} \tag{6}$$

with $\mu_{10} = \mathrm{E}\{U_1|H_0\}$ given by (4a), $\sigma_{10}^2 = \mathrm{Var}\{U_1|H_0\}$ given by (4b), $\mu_{11} = \mathrm{E}\{U_1|H_1\}$ given by (4c), and $\sigma_{11}^2 = \mathrm{Var}\{U_1|H_1\}$ given by (4d), by matching the mean and variance of U_1 with those of a Gaussian distribution. Thus, using (5) and (6), the IED is derived as

$$U_1 \underset{H_1}{\overset{H_0}{\gtrless}} T_{1\mathrm{IED}}, \; |h_0|^2 > |h_1|^2 \tag{7a}$$

$$U_1 \underset{H_1}{\overset{H_0}{\lessgtr}} T_{1\mathrm{IED}}, \; |h_0|^2 < |h_1|^2 \tag{7b}$$

where $T_{1\mathrm{IED}}$ is the detection threshold determined by the larger root of the second-order polynomial

$$\left(\frac{1}{2\sigma_{11}^2} - \frac{1}{2\sigma_{10}^2}\right)x^2 + \left(\frac{\mu_{10}}{\sigma_{10}^2} - \frac{\mu_{11}}{\sigma_{11}^2}\right)x + \ln\frac{\sigma_{11}^2}{\sigma_{10}^2} = 0 \tag{8}$$

since $(\mu_{10}^2/2\sigma_{10}^2) = (\mu_{11}^2/2\sigma_{11}^2)$. This gives $T_{1\mathrm{IED}} = (1/2a_1)(-b_1 + \sqrt{b_1^2 - 4a_1c_1})$, where $a_1 = (1/2\sigma_{11}^2) - (1/2\sigma_{10}^2)$, $b_1 = (\mu_{10}/\sigma_{10}^2) - (\mu_{11}/\sigma_{11}^2)$ and $c_1 = \ln(\sigma_{11}^2/\sigma_{10}^2)$. The BER of the IED can be approximated as

$$\begin{aligned} P_e &\approx \frac{1}{2}\int_{-\infty}^{T_{1\mathrm{IED}}} f(U_1|H_0)dR + \frac{1}{2}\int_{T_{1\mathrm{IED}}}^{\infty} f(U_1|H_1)dR \\ &= \frac{1}{2}\left[1 - Q\left(\frac{T_{1\mathrm{IED}} - \mu_{10}}{\sigma_{10}}\right) + Q\left(\frac{T_{1\mathrm{IED}} - \mu_{11}}{\sigma_{11}}\right)\right] \end{aligned} \tag{9}$$

for $|h_0|^2 > |h_1|^2$ and

$$\begin{aligned} P_e &\approx \frac{1}{2}\int_{T_{1\mathrm{IED}}}^{\infty} f(U_1|H_0)dR + \frac{1}{2}\int_{-\infty}^{T_{1\mathrm{IED}}} f(U_1|H_1)dR \\ &= \frac{1}{2}\left[Q\left(\frac{T_{1\mathrm{IED}} - \mu_{10}}{\sigma_{10}}\right) + 1 - Q\left(\frac{T_{1\mathrm{IED}} - \mu_{11}}{\sigma_{11}}\right)\right] \end{aligned} \tag{10}$$

for $|h_0|^2 < |h_1|^2$, where $G(\cdot)$ is the standard Gaussian Q function [47, eq. (2-1-97)]. Note that the above detector is similar to that proposed in [44], except that here it is used for an AmBC signal with the cascaded Gaussian random variables while in [44] it was used for a pure Gaussian random signal. Thus, the statistics of the decision variables are totally different and the above derivation is new.

3) Energy Detector: It can be shown that the energy detector in this case is equivalent to the ML detector. Indeed, the test statistic in the ML detector is actually the energy of the received signal $Z_1 = ||\mathbf{y}||^2 = \sum_{n=1}^{N} |y[n]|^2$ [18, eq. (8)]. This is the only case in the work where the energy detector is equivalent to the ML detector. For clarification, all the energy detectors and ML detectors in the following sections refer to different detectors and are not used interchangeably.

4) Magnitude Detector: Denote $R_1 = \sum_{n=1}^{N} |y[n]|$ as the test statistic for the magnitude detector. As discussed before, it is a special case of the IED when $p = 1$. Thus, one can derive a magnitude detector using the Gaussian approximation by letting $p = 1$ in the results for IED. Alternatively, one may also use the Nakagami-m approximation. By letting $p = 1$ in (4), one has the mean and variance of R_1 as

$$\mathrm{E}\{R_1|H_0\} = N\frac{\sqrt{\pi}}{2}\sqrt{|h_0|^2P_s + \sigma_w^2} \tag{11a}$$

$$\mathrm{Var}\{R_1|H_0\} = N\left(1 - \frac{\pi}{4}\right)\left(|h_0|^2P_s + \sigma_w^2\right) \tag{11b}$$

$$\mathrm{E}\{R_1|H_1\} = N\frac{\sqrt{\pi}}{2}\sqrt{|h_1|^2P_s + \sigma_w^2} \tag{11c}$$

$$\mathrm{Var}\{R_1|H_1\} = N\left(1 - \frac{\pi}{4}\right)\left(|h_1|^2P_s + \sigma_w^2\right). \tag{11d}$$

If the Nakagami-m approximation is used, one has

$$f(R_1|H_0) \approx \frac{2m_0^{m_0}R^{2m_0-1}}{\Gamma(m_0)\Omega_0^{m_0}}e^{-\frac{m_0}{\Omega_0}R^2} \tag{12}$$

and

$$f(R_1|H_1) \approx \frac{2m_1^{m_1}R^{2m_1-1}}{\Gamma(m_1)\Omega_1^{m_1}}e^{-\frac{m_1}{\Omega_1}R^2} \tag{13}$$

with $\Omega_0 = \mathrm{Var}\{R_1|H_0\} + \mathrm{E}^2\{R_1|H_0\} = [N + (\pi/4)N(N-1)][|h_0|^2P_s + \sigma_w^2]$ and m_0 is determined by $(\Gamma(m_0+0.5)/\Gamma(m_0)\sqrt{m_0}) = (N\sqrt{\pi/4}/\sqrt{N+N(N-1)\pi/4})$ from (11a) and (11b), $\Omega_1 = \mathrm{Var}\{R_1|H_1\} + \mathrm{E}^2\{R_1|H_1\} = [N + (\pi/4)N(N-1)][|h_1|^2P_s + \sigma_w^2]$ and m_1 is determined by $(\Gamma(m_1+0.5)/\Gamma(m_1)\sqrt{m_1}) = (N\sqrt{\pi/4}/\sqrt{N+N(N-1)\pi/4})$ from (11c) and (11d), by matching the first- and second-order moments of R_1 with those of a Nakagami-m distribution. Thus, the magnitude detector using the Nakagami approximation is derived from (12) and (13) as

$$R_1 \underset{H_1}{\overset{H_0}{\gtrless}} T_{1MDNak}, \ |h_0|^2 > |h_1|^2 \tag{14a}$$

$$R_1 \underset{H_1}{\overset{H_0}{\lessgtr}} T_{1MDNak}, \ |h_0|^2 < |h_1|^2 \tag{14b}$$

where

$$T_{1MDNak} = \sqrt{\frac{\Omega_0\Omega_1}{\Omega_0 - \Omega_1}\ln\frac{\Omega_0}{\Omega_1}}. \tag{15}$$

The BER of the magnitude detector using the Nakagami-m approximation can be derived from (14) as

$$P_e \approx \frac{1}{2\Gamma(m_0)}\left[\gamma\left(m_0, \frac{m_0T_{1MDNak}^2}{\Omega_0}\right) + \Gamma\left(m_1, \frac{m_1T_{1MDNak}^2}{\Omega_1}\right)\right] \tag{16}$$

for $|h_0|^2 > |h_1|^2$ and

$$P_e \approx \frac{1}{2\Gamma(m_0)}\left[\Gamma\left(m_0, \frac{m_0T_{1MDNak}^2}{\Omega_0}\right) + \gamma\left(m_1, \frac{m_1T_{1MDNak}^2}{\Omega_1}\right)\right] \tag{17}$$

for $|h_0|^2 < |h_1|^2$, as $m_0 = m_1$.

B. Coherent Detection for PSK Ambient Signals

In this case, all of h_{sr}, h_{tr}, and h_{st} or both h_0 and h_1 are still known to perform coherent detection, but the ambient signal is PSK modulated with $s[n] = \sqrt{P_s}e^{j\theta_n}$, where $\theta_n \in \{0, (2\pi/M), \ldots, (2\pi(M-1)/M)\}$ randomly chosen from an M-ary PSK (MPSK). PSK was also considered in [18] and [20]. However, they used the energy detector directly without further investigation. This work will extend their detectors to the optimal detectors.

Since θ_n is unknown, one needs to remove the phase information from the received signal as

$$|y[n]| = |h_{sr}\sqrt{P_s} + \eta h_{tr}h_{st}\sqrt{P_s}d + w'[n]| \tag{18}$$

where $w'[n] = w[n]e^{-j\theta_n}$ with $w'[n] \sim \mathcal{CN}(0, \sigma_w^2)$, as the phase shift does not change the Gaussian distribution. Thus, the detectors here using $|y[n]|$ are only applicable to PSK. It is not a general assumption for all signals. For example, for quadrature amplitude modulation, its amplitude information cannot be removed by squaring, which would lead to a mixture of Rician with different variances for the sample distribution.

1) ML Detector: From (18), the sample $|y[n]|$ follows a Rician distribution. Thus, the likelihood function or the joint PDF of all samples in H_0 and H_1 can be derived as

$$f(\mathbf{y}|H_0) = \frac{\prod_{n=1}^{N}|y[n]|}{\left(\sigma_w^2/2\right)^N}e^{-\frac{\sum_{n=1}^{N}|y[n]|^2}{\sigma_w^2} - \frac{N|h_0|^2P_s}{\sigma_w^2}} \prod_{n=1}^{N} I_0\left(\frac{|y[n]||h_0\sqrt{P_s}|}{\sigma_w^2/2}\right) \tag{19}$$

and

$$f(\mathbf{y}|H_1) = \frac{\prod_{n=1}^{N}|y[n]|}{\left(\sigma_w^2/2\right)^N}e^{-\frac{\sum_{n=1}^{N}|y[n]|^2}{\sigma_w^2} - \frac{N|h_1|^2P_s}{\sigma_w^2}} \prod_{n=1}^{N} I_0\left(\frac{|y[n]||h_1\sqrt{P_s}|}{\sigma_w^2/2}\right) \tag{20}$$

where $I_0(\cdot)$ is the zeroth order modified Bessel function of the first type [48, eq. (8.406.1)]. By taking the log-likelihood ratio

of (19) to (20) and after some manipulations, one has the ML detector in this case as

$$\sum_{n=1}^{N} \ln \frac{I_0\left(\frac{|y[n]||h_0\sqrt{P_s}|}{\sigma_w^2/2}\right)}{I_0\left(\frac{|y[n]||h_1\sqrt{P_s}|}{\sigma_w^2/2}\right)} \underset{H_1}{\overset{H_0}{\gtrless}} T_{2ML} \tag{21}$$

with

$$T_{2ML} = \frac{NP_s}{\sigma_w^2}\left(|h_0|^2 - |h_1|^2\right). \tag{22}$$

To the best of the author's knowledge, this is a new detector that has not been derived in the literature. Since $\ln I_0(x) \approx |x|$ when x is large and $\ln I_0(x) \approx x^2$ when x is small, it actually includes the magnitude detector and the energy detector as special cases for large and small signal-to-noise ratios (SNRs), respectively. Thus, it is possible to approximate the Bessel function but the approximation will lead to other detectors.

2) IED: Next, we will derive the IED using the Gaussian approximation. For the IED, the test statistic is $U_2 = \sum_{n=1}^{N} |y[n]|^p$, where $|y[n]|$ is given by (18). This sum does not have a closed-form expression for its PDF. Thus, we will use approximations based on moment-matching again.

Using [47, eq. (2-1-146)], the mean and variance of U_2 can be derived as

$$\mathrm{E}\{U_2|H_0\} = N\left(\sigma_w^2\right)^{\frac{p}{2}}\Gamma\left(1+\frac{p}{2}\right)L_{\frac{p}{2}}\left(-|h_0|^2P_s/\sigma_w^2\right) \tag{23a}$$

$$\mathrm{Var}\{U_2|H_0\} = N\sigma_w^{2p}\Big[\Gamma(1+p)L_p\left(-|h_0|^2P_s/\sigma_w^2\right) - \Gamma^2\left(1+\frac{p}{2}\right)L_{\frac{1}{2}}^2\left(-|h_0|^2P_s/\sigma_w^2\right)\Big] \tag{23b}$$

$$\mathrm{E}\{U_2|H_1\} = N\left(\sigma_w^2\right)^{\frac{p}{2}}\Gamma\left(1+\frac{p}{2}\right)L_{\frac{p}{2}}\left(-|h_1|^2P_s/\sigma_w^2\right) \tag{23c}$$

$$\mathrm{Var}\{U_2|H_1\} = N\sigma_w^{2p}\Big[\Gamma(1+p)L_p\left(-|h_1|^2P_s/\sigma_w^2\right) -\Gamma^2\left(1+\frac{p}{2}\right)L_{\frac{1}{2}}^2\left(-|h_1|^2P_s/\sigma_w^2\right)\Big] \tag{23d}$$

where $L(\cdot)$ is the Laguerre polynomial with $L_k(x) = e^{-x}{}_1F_1(1+k,1;x)$ and ${}_1F_1(\cdot,\cdot;\cdot)$ is the confluent hypergeometric function [48, eq. (9.201)].

Thus, if one uses the Gaussian approximation, one has the PDFs of U_2 given by

$$f(U_2|H_0) \approx \frac{1}{\sqrt{2\pi\sigma_{20}^2}} e^{-\frac{(U_2-\mu_{20})^2}{2\sigma_{20}^2}} \tag{24}$$

and

$$f(U_2|H_1) \approx \frac{1}{\sqrt{2\pi\sigma_{21}^2}} e^{-\frac{(U_2-\mu_{21})^2}{2\sigma_{21}^2}} \tag{25}$$

with $\mu_{20} = \mathrm{E}\{U_2|H_0\}$ from (23a), $\sigma_{20}^2 = \mathrm{Var}\{U_2|H_0\}$ from (23b), $\mu_{21} = \mathrm{E}\{U_2|H_1\}$ from (23c), and $\sigma_{21}^2 = \mathrm{Var}\{U_2|H_1\}$ from (23d). Using (24) and (25), the IED is derived as

$$U_2 \underset{H_1}{\overset{H_0}{\gtrless}} T_{2\mathrm{IED}}, \; |h_0|^2 > |h_1|^2 \tag{26a}$$

$$U_2 \underset{H_1}{\overset{H_0}{\lessgtr}} T_{2\mathrm{IED}}, \; |h_0|^2 < |h_1|^2 \tag{26b}$$

where $T_{2\mathrm{IED}}$ is the larger root of the second-order polynomial

$$\left(\frac{1}{2\sigma_{21}^2} - \frac{1}{2\sigma_{20}^2}\right)x^2 + \left(\frac{\mu_{20}}{\sigma_{20}^2} - \frac{\mu_{21}}{\sigma_{21}^2}\right)x + \frac{\mu_{21}^2}{2\sigma_{21}^2} - \frac{\mu_{20}^2}{2\sigma_{20}^2} + \ln\frac{\sigma_{21}^2}{\sigma_{20}^2} = 0 \tag{27}$$

as $T_{2\mathrm{IED}} = (1/2a_2)(-b_2 + \sqrt{b_2^2 - 4a_2c_2})$, $a_2 = (1/2\sigma_{21}^2) - (1/2\sigma_{20}^2)$, $b_2 = (\mu_{20}/\sigma_{20}^2) - (\mu_{21}/\sigma_{21}^2)$ and $c_2 = (\mu_{21}^2/2\sigma_{21}^2) - (\mu_{20}^2/2\sigma_{20}^2) + \ln(\sigma_{21}^2/\sigma_{20}^2)$. Similarly, the BER can be approximated as

$$P_e \approx \frac{1}{2}\left[1 - Q\left(\frac{T_{2\mathrm{IED}} - \mu_{20}}{\sigma_{20}}\right) + Q\left(\frac{T_{2\mathrm{IED}} - \mu_{21}}{\sigma_{21}}\right)\right] \tag{28}$$

for $|h_0|^2 > |h_1|^2$ and

$$P_e \approx \frac{1}{2}\left[Q\left(\frac{T_{2\mathrm{IED}} - \mu_{20}}{\sigma_{20}}\right) + 1 - Q\left(\frac{T_{2\mathrm{IED}} - \mu_{21}}{\sigma_{21}}\right)\right] \tag{29}$$

for $|h_0|^2 < |h_1|^2$.

3) Energy Detector: The energy detector could be obtained by letting $p = 2$ in the results for IED using the Gaussian approximation, which leads to the energy detector proposed in [18] and [20]. However, better energy detection can also be derived as follows.

For the energy detector, the test statistic is $Z_2 = \sum_{n=1}^{N} |y[n]|^2$, where $|y[n]|$ is given by (18). From (18), since $|y[n]|$ is a Rician random variable, Z_2 follows a noncentral χ^2 distribution. Thus, the PDFs of Z_2 in H_0 and H_1 are derived as

$$f(Z_2|H_0) = \frac{1}{\sigma_w^2}\left(\frac{Z_2}{N|h_0|^2P_s}\right)^{\frac{N-1}{2}} e^{-\frac{N|h_0|^2P_s+Z_2}{\sigma_w^2}} \times I_{N-1}\left(\frac{\sqrt{Z_2N|h_0|^2P_s}}{\sigma_w^2/2}\right) \tag{30}$$

and

$$f(Z_2|H_1) = \frac{1}{\sigma_w^2}\left(\frac{Z_2}{N|h_1|^2P_s}\right)^{\frac{N-1}{2}} e^{-\frac{N|h_1|^2P_s+Z_2}{\sigma_w^2}} \times I_{N-1}\left(\frac{\sqrt{Z_2N|h_1|^2P_s}}{\sigma_w^2/2}\right) \tag{31}$$

respectively, where $I_{N-1}(\cdot)$ is the $(N-1)$th order modified Bessel function of the first type.

Then, by taking the log-likelihood ratio of $f(Z_2|H_0)$ in (30) to $f(Z_2|H_1)$ in (31) and after some manipulations, one can

derive the optimum energy detector as

$$\ln I_{N-1}\left(\frac{|h_0|\sqrt{NP_sZ_2}}{\sigma_w^2/2}\right) - \ln I_{N-1}\left(\frac{|h_1|\sqrt{NP_sZ_2}}{\sigma_w^2/2}\right) \underset{H_1}{\overset{H_0}{\gtrless}} C \tag{32}$$

where $C = (N-1)\ln(|h_0|/|h_1|) + (NP_s/\sigma_w^2)(|h_0|^2 - |h_1|^2)$. Solving the inequality for Z_2, (32) is equivalent to

$$Z_2 \underset{H_1}{\overset{H_0}{\gtrless}} T_{2ED}, \; |h_0|^2 > |h_1|^2 \tag{33a}$$

$$Z_2 \underset{H_1}{\overset{H_0}{\lessgtr}} T_{2ED}, \; |h_0|^2 < |h_1|^2 \tag{33b}$$

where T_{2ED} is the solution to the equation

$$\ln I_{N-1}\left(\frac{\sqrt{xN|h_0|^2P_s}}{\sigma_w^2/2}\right) - \ln I_{N-1}\left(\frac{\sqrt{xN|h_1|^2P_s}}{\sigma_w^2/2}\right) = (N-1)\ln\frac{|h_0|}{|h_1|} + \frac{NP_s}{\sigma_w^2}\left(|h_0|^2 - |h_1|^2\right) \tag{34}$$

for x by equating (30) and (31). This equation is nonlinear and the solution has no closed form but can be obtained using MATLAB or iteration. There is no good approximation to the Bessel function $I_{N-1}(\cdot)$. Also, using (30) and (31) in (33), the BER of this energy detector is derived as

$$P_e = \frac{1}{2}\left[1 - Q_N\left(\sqrt{2NP_s|h_0|^2/\sigma_w^2}, \sqrt{2T_{2ED}/\sigma_w^2}\right) + Q_N\left(\sqrt{2NP_s|h_1|^2/\sigma_w^2}, \sqrt{2T_{2ED}/\sigma_w^2}\right)\right] \tag{35}$$

for $|h_0|^2 > |h_1|^2$ and

$$P_e = \frac{1}{2}\left[Q_N\left(\sqrt{2NP_s|h_0|^2/\sigma_w^2}, \sqrt{2T_{2ED}/\sigma_w^2}\right) + 1 - Q_N\left(\sqrt{2NP_s|h_1|^2/\sigma_w^2}, \sqrt{2T_{2ED}/\sigma_w^2}\right)\right] \tag{36}$$

for $|h_0|^2 < |h_1|^2$, where $Q_N(\cdot,\cdot)$ is the Nth order generalized Marcum Q function [47, eq. (2-1-122)].

4) Magnitude Detector: For the magnitude detector, the test statistic is $R_2 = \sum_{n=1}^{N}|y[n]|$, where $|y[n]|$ is given by (18). Thus, it can be obtained by letting $p = 1$ in the IED using the Gaussian approximation.

C. Partial Coherent Detection for Gaussian Signals

In this case, the values of h_{sr} or h_0 are known but the values of h_{st} and h_{tr} or h_1 are unknown. This is the case when the tag reader is able to estimate the SR link by taking advantage of known pilots from the ambient source but the tag cannot perform such estimation or send any pilots due to its limited capability. Then, partial coherent detection is performed at the tag reader. In [25], none of h_{sr}, h_{st}, and h_{tr} was known so that noncoherent detection was used. Assume that the ambient signal is a Gaussian distributed with $s[n] \sim \mathcal{CN}(0, P_s)$. Also, similar to [25], assume $h_{st} \sim \mathcal{CN}(0, \sigma_{st}^2)$ and $h_{tr} \sim \mathcal{CN}(0, \sigma_{tr}^2)$.

1) ML Detector: Since $h_1 = h_{sr} + \eta h_{st}h_{tr}$, conditioned on h_{st}, $|h_1|^2$ is noncentral χ^2 distributed with

$$f_{|h_1|^2}(t|h_{st}) = \frac{1}{\eta^2|h_{st}|^2\sigma_{tr}^2} e^{-\frac{t+|h_{sr}|^2}{\eta^2|h_{st}|^2\sigma_{tr}^2}} I_0\left(\frac{2\sqrt{t}|h_{sr}|}{\eta^2|h_{st}|^2\sigma_{tr}^2}\right). \tag{37}$$

Then, since $|h_{st}|^2$ is exponentially distributed, one has the unconditional PDF of $|h_1|^2$ as

$$f_{|h_1|^2}(t) = \int_0^\infty \frac{1}{\eta^2\sigma_{st}^2\sigma_{tr}^2 x} e^{-\frac{t+|h_{sr}|^2}{\eta^2\sigma_{tr}^2 x} - \frac{x}{\sigma_{st}^2}} I_0\left(\frac{2\sqrt{t}|h_{sr}|}{\eta^2\sigma_{tr}^2 x}\right) dx = \frac{1}{\eta^2\sigma_{st}^2\sigma_{tr}^2} E\left(\frac{t+|h_{sr}|^2}{2\sqrt{t}|h_{sr}|}, \frac{2\sqrt{t}|h_{sr}|}{\eta^2\sigma_{tr}^2\sigma_{st}^2}\right) \tag{38}$$

where $E(a,b) = \int_0^\infty (I_0(r)/r)e^{-ar-(b/r)}dr$. Thus, the likelihood function for H_0 is the same as coherent detection but the likelihood function for H_1 becomes

$$f(\mathbf{y}|H_1) = \int_0^\infty \frac{e^{-\frac{\|\mathbf{y}\|^2}{tP_s+\sigma_w^2}} E\left(\frac{t+|h_{sr}|^2}{2\sqrt{t}|h_{sr}|}, \frac{2\sqrt{t}|h_{sr}|}{\eta^2\sigma_{tr}^2\sigma_{st}^2}\right)}{\eta^2\sigma_{st}^2\sigma_{tr}^2\left[\pi\left(tP_s+\sigma_w^2\right)\right]^N} dt. \tag{39}$$

This integral cannot be solved so one has to use (39) directly and the likelihood function for H_0 in [18] to calculate the likelihood ratio. The complexity of this detector is similar to those in [25]. Next, we will derive the IED.

2) IED: For the IED, in order to use the Gaussian approximation, we need to derive the mean and variance of $U_3 = \sum_{n=1}^{N}|y[n]|^p$. From (4), one can calculate the unconditional mean and variance in H_0 and the conditional mean and variance in H_1 as

$$\mathrm{E}\{U_3|H_0\} = N\left(|h_{sr}|^2P_s + \sigma_w^2\right)^{\frac{p}{2}}\Gamma\left(1+\frac{p}{2}\right) \tag{40a}$$

$$\mathrm{Var}\{U_3|H_0\} = N\left[\Gamma(1+p) - \Gamma^2\left(1+\frac{p}{2}\right)\right]\left(|h_{sr}|^2P_s + \sigma_w^2\right)^p \tag{40b}$$

$$\mathrm{E}\{U_3|H_1, h_1\} = N\left(|h_1|^2P_s + \sigma_w^2\right)^{\frac{p}{2}}\Gamma\left(1+\frac{p}{2}\right) \approx N\Gamma\left(1+\frac{p}{2}\right)\left[\left(|h_1|^2P_s\right)^{\frac{p}{2}} + \frac{p}{2}\sigma_w^2\left(|h_1|^2P_s\right)^{\frac{p}{2}-1}\right] \tag{40c}$$

$$\mathrm{Var}\{U_3|H_1, h_1\} = N\left[\Gamma(1+p) - \Gamma^2\left(1+\frac{p}{2}\right)\right] \times \left(|h_1|^2P_s + \sigma_w^2\right)^p \approx N\left[\Gamma(1+p) - \Gamma^2\left(1+\frac{p}{2}\right)\right] \times \left[\left(|h_1|^2P_s\right)^p + p\sigma_w^2\left(|h_1|^2P_s\right)^{p-1}\right] \tag{40d}$$

where the approximation in (40c) and (40d) is obtained by using $(1+x)^a \approx 1+ax$ when x is small. The PDF of $|h_1|^2$ is given in (38). Thus, the unconditional mean and variance of U_3 in H_1 are

$$\mathrm{E}\{U_3|H_1\} \approx N\Gamma\left(1+\frac{p}{2}\right)P_s^{\frac{p}{2}-1}\left[P_sD_1 + \frac{p}{2}\sigma_w^2D_2\right] \tag{41a}$$

$$\mathrm{Var}\{U_3|H_1\} \approx N\left[\Gamma(1+p) - \Gamma^2\left(1+\frac{p}{2}\right)\right]P_s^{p-1}\left[P_sD_3 + p\sigma_w^2D_4\right] \tag{41b}$$

where

$$D_1 = \int_0^\infty \frac{\beta I_0(r)}{|h_{sr}|^2 r}\left(\frac{|h_{sr}|^2 r}{r+\frac{\beta}{r}}\right)^{\frac{p}{2}+1} K_{p+2}\left(\sqrt{r^2+\beta}\right)dr \tag{42}$$

$$D_2 = \int_0^\infty \frac{\beta I_0(r)}{|h_{sr}|^2 r}\left(\frac{|h_{sr}|^2 r}{r+\frac{\beta}{r}}\right)^{\frac{p}{2}} K_p\left(\sqrt{r^2+\beta}\right)dr \quad (43)$$

$$D_3 = \int_0^\infty \frac{\beta I_0(r)}{|h_{sr}|^2 r}\left(\frac{|h_{sr}|^2 r}{r+\frac{\beta}{r}}\right)^{p+1} K_{2p+2}\left(\sqrt{r^2+\beta}\right)dr \quad (44)$$

$$D_4 = \int_0^\infty \frac{\beta I_0(r)}{|h_{sr}|^2 r}\left(\frac{|h_{sr}|^2 r}{r+\frac{\beta}{r}}\right)^{p} K_{2p}\left(\sqrt{r^2+\beta}\right)dr \quad (45)$$

with $\beta = (4|h_{sr}|^2/\eta^2\sigma_{tr}^2\sigma_{st}^2)$, $K(\cdot)$ being the modified Bessel function of the second type [48, eq. (8.407)], and [48, eq. (3.478.4)] being used to solve the integrations for (42)–(45). Otherwise, they would contain a 2-D integral. Then, the IED is derived as

$$U_3 \underset{H_1}{\overset{H_0}{\gtrless}} T_{3\text{IED}}, \quad |h_0|^2 > |h_1|^2 \quad (46a)$$

$$U_3 \underset{H_1}{\overset{H_0}{\lessgtr}} T_{3\text{IED}}, \quad |h_0|^2 < |h_1|^2 \quad (46b)$$

where $T_{3\text{IED}}$ is the larger root of the second-order polynomial

$$\left(\frac{1}{2\sigma_{31}^2}-\frac{1}{2\sigma_{30}^2}\right)x^2 + \left(\frac{\mu_{30}}{\sigma_{30}^2}-\frac{\mu_{31}}{\sigma_{31}^2}\right)x + \frac{\mu_{31}^2}{2\sigma_{31}^2}-\frac{\mu_{30}^2}{2\sigma_{30}^2}+\ln\frac{\sigma_{31}^2}{\sigma_{30}^2}=0 \quad (47)$$

as $T_{3\text{IED}} = (1/2a_3)(-b_3+\sqrt{b_3^2-4a_3c_3})$, where $a_3 = (1/2\sigma_{31}^2)-(1/2\sigma_{30}^2)$, $b_3 = (\mu_{30}/\sigma_{30}^2)-(\mu_{31}/\sigma_{31}^2)$ and $c_3 = (\mu_{31}^2/2\sigma_{31}^2)-(\mu_{30}^2/2\sigma_{30}^2)+\ln(\sigma_{31}^2/\sigma_{30}^2)$ and m_{30}, σ_{30}^2, m_{31}, σ_{31}^2 are determined by (40a), (40b), (41a), and (41b), respectively.

By letting $p = 1$ and $p = 2$ in the above results, the magnitude detector and energy detector using the Gaussian approximation can be derived, respectively. These results are not given here to make this article compact.

D. Partial Coherent Detection for PSK Ambient Signals

In the last case, h_{st} and h_{tr} or h_1 are still unknown to perform partial coherent detection but the ambient signal is PSK modulated with $s[n] = \sqrt{P_s}e^{j\theta_n}$, where θ_n is unknown. Thus, one can use the absolute value of $y[n]$ to remove the phase information as in (18).

1) ML Detector: The likelihood function in H_0 is still given by (19), as $h_0 = h_{sr}$ is known. However, the likelihood function in H_1 is calculated by using (20) and (38) as

$$f(\mathbf{y}|H_1) = \frac{\prod_{n=1}^N |y[n]|}{(\sigma_w^2/2)^N} e^{-\frac{\sum_{n=1}^N |y[n]|^2}{\sigma_w^2}} \int_0^\infty e^{-\frac{NP_s t}{\sigma_w^2}} \prod_{n=1}^N I_0\left(\frac{|y[n]|\sqrt{P_s t}}{\sigma_w^2/2}\right)\frac{E\left(\frac{t+|h_{sr}|^2}{2\sqrt{t}|h_{sr}|}, \frac{2\sqrt{t}|h_{sr}|}{\eta^2\sigma_{tr}^2\sigma_{st}^2}\right)}{\eta^2\sigma_{st}^2\sigma_{tr}^2}dt. \quad (48)$$

This integral is difficult to solve so one has to use (19) and (48) to calculate the likelihood ratio directly for the ML detection, with similar complexity to those in [25] for noncoherent detection. Next, we will derive the IED using the Gaussian approximation.

2) IED: For the IED in this case, the mean and variance of the test statistic $U_4 = \sum_{n=1}^N |y[n]|^p$ can be derived as

$$\mathrm{E}\{U_4|H_0\} = N\left(\sigma_w^2\right)^{\frac{p}{2}}\Gamma\left(1+\frac{p}{2}\right)L_{\frac{p}{2}}\left(-|h_{sr}|^2P_s/\sigma_w^2\right) \quad (49a)$$

$$\mathrm{Var}\{U_4|H_0\} = N\sigma_w^{2p}\Big[\Gamma(1+p)L_p\left(-|h_{sr}|^2P_s/\sigma_w^2\right) - \Gamma^2\left(1+\frac{p}{2}\right)L_{\frac{1}{2}}^2\left(-|h_{sr}|^2P_s/\sigma_w^2\right)\Big] \quad (49b)$$

$$\mathrm{E}\{U_4|H_1\} = N\left(\sigma_w^2\right)^{\frac{p}{2}}\Gamma\left(1+\frac{p}{2}\right)\int_0^\infty \frac{L_{\frac{p}{2}}\left(-tP_s/\sigma_w^2\right)}{\eta^2\sigma_{st}^2\sigma_{tr}^2} \cdot E\left(\frac{t+|h_{sr}|^2}{2\sqrt{t}|h_{sr}|}, \frac{2\sqrt{t}|h_{sr}|}{\eta^2\sigma_{tr}^2\sigma_{st}^2}\right)dt \quad (49c)$$

$$\mathrm{Var}\{U_4|H_1\} = \frac{N\sigma_w^{2p}}{\eta^2\sigma_{st}^2\sigma_{tr}^2}\Big[\Gamma(1+p)\int_0^\infty L_p\left(-tP_s/\sigma_w^2\right) \cdot E\left(\frac{t+|h_{sr}|^2}{2\sqrt{t}|h_{sr}|}, \frac{2\sqrt{t}|h_{sr}|}{\eta^2\sigma_{tr}^2\sigma_{st}^2}\right)dt - \Gamma^2\left(1+\frac{p}{2}\right)\int_0^\infty L_{\frac{1}{2}}^2\left(-tP_s/\sigma_w^2\right) \cdot E\left(\frac{t+|h_{sr}|^2}{2\sqrt{t}|h_{sr}|}, \frac{2\sqrt{t}|h_{sr}|}{\eta^2\sigma_{tr}^2\sigma_{st}^2}\right)dt\Big] \quad (49d)$$

by using (23) and (38). Similarly, the IED is derived as

$$U_4 \underset{H_1}{\overset{H_0}{\gtrless}} T_{4\text{IED}}, \quad |h_0|^2 > |h_1|^2 \quad (50a)$$

$$U_4 \underset{H_1}{\overset{H_0}{\lessgtr}} T_{4\text{IED}}, \quad |h_0|^2 < |h_1|^2 \quad (50b)$$

where $T_{4\text{IED}}$ is the larger root of the second-order polynomial

$$\left(\frac{1}{2\sigma_{41}^2}-\frac{1}{2\sigma_{40}^2}\right)x^2 + \left(\frac{\mu_{40}}{\sigma_{40}^2}-\frac{\mu_{41}}{\sigma_{41}^2}\right)x + \frac{\mu_{41}^2}{2\sigma_{41}^2}-\frac{\mu_{40}^2}{2\sigma_{40}^2}+\ln\frac{\sigma_{41}^2}{\sigma_{40}^2}=0 \quad (51)$$

as $T_{4\text{IED}} = (1/2a_4)(-b_4+\sqrt{b_4^2-4a_4c_4})$, where $a_4 = (1/2\sigma_{41}^2)-(1/2\sigma_{40}^2)$, $b_4 = (\mu_{40}/\sigma_{40}^2)-(\mu_{41}/\sigma_{41}^2)$ and $c_4 = (\mu_{41}^2/2\sigma_{41}^2)-(\mu_{40}^2/2\sigma_{40}^2)+\ln(\sigma_{41}^2/\sigma_{40}^2)$ and m_{40}, σ_{40}^2, m_{41}, σ_{41}^2 are determined by (49a)–(49d), respectively. For magnitude detection and energy detection using the Gaussian approximation, one can set $p = 1$ and $p = 2$, respectively, in the above results.

Note that the coherent detectors in Sections III-A and III-B require the channel state information of $|h_0|^2$ and $|h_1|^2$, while the partial coherent detectors in Sections III-C and III-D require the channel state information of $|h_0|^2$. Efficient "semi-blind" estimators for $|h_0|^2$ and $|h_1|^2$ have been given in [18, Sec. IV], where $|h_0|^2$ and $|h_1|^2$ were first estimated blindly and then discriminated using training symbols. Alternatively, moment-based estimators may be applied to the received signal in (3) to estimate them blindly [49], [50]. For example,

Algorithm 1 Backscatter Signal Detection Algorithm

Require: received signals $y[n]$, $(k = 1, ..., K)$

Initialization: calculate $\sum_{n=1}^{N} |y[n]|^p$, $\sum_{n=1}^{N} |y[n]|^2$, $\sum_{n=1}^{N} |y[n]|$
if coherent detection for Gaussian signals **then**
  if maximum likelihood or energy detection **then**
    Use [19, eq. (8)];
  else if improved energy detection **then**
    Calculate μ_{10}, σ_{10}^2, μ_{11}, σ_{11}^2 using (4a)–(4d);
    Calculate $T_{1\text{IED}}$ using (8);
    Perform the detection using (7).
  else if magnitude detection **then**
    Calculate m_0, Ω_0, m_1, Ω_1 using (11a)–(11d);
    Calculate T_{1MDNak} using (15);
    Perform the detection using (14).
  end if
else if coherent detection for PSK signals **then**
  if maximum likelihood detection **then**
    Calculate T_{2ML} using (22);
    Perform the detection using (21).
  else if improved energy or magnitude detection **then**
    Calculate μ_{20}, σ_{20}^2, μ_{21}, σ_{21}^2 using (23a)–(23d);
    Calculate $T_{2\text{IED}}$ using (27);
    Perform the detection using (26).
  else if energy detection **then**
    Calculate T_{2ED} using (34);
    Perform the detection using (33).
  end if
else if partial coherent detection for Gaussian signals **then**
  if improved energy, energy, or magnitude detection **then**
    Calculate μ_{30}, σ_{30}^2, μ_{31}, σ_{31}^2 using (40a), (40b), (41a), (41b);
    Calculate T_{3IED} using (47);
    Perform the detection using (46).
  end if
else if partial coherent detection for PSK signals **then**
  if improved energy, energy, or magnitude detection **then**
    Calculate μ_{40}, σ_{40}^2, μ_{41}, σ_{41}^2 using (49a)–(49d);
    Calculate T_{3IED} using (51);
    Perform the detection using (50).
  end if
end if

the second-order and fourth-order moments of (3) can be calculated, based on which $|h_0|^2$ and $|h_1|^2$ can be estimated. One may also let the tag send a series of "0" or stop transmission to estimate $|h_{sr}|^2$ or $|h_0|^2$ at the tag reader for partial coherent detection. Since the focus of this article is on signal detection, we assume that the channel state information is available and will not discuss its estimation further. All detectors are summarized in Algorithm 1.

IV. Numerical Results and Discussion

In this section, numerical examples are presented to show the BER performances of the derived detectors. For convenience, define $\gamma = (P_s/\sigma_w^2)$ and $\beta = (\eta^2\sigma_{tr}^2\sigma_{st}^2/\sigma_{sr}^2)$ to represent the signal quality. The actual signal-to-noise ratio at the receiver also depends on the channel gains. In the examples, we set $\sigma_w^2 = 1$, $\sigma_{tr}^2 = 1$, $\sigma_{st}^2 = 1$, and $\eta = 1$ for illustration purposes only, while P_s and σ_{sr}^2 change with γ and β, respectively. Other values can also be used. For example, we can set η to be less than 1, which is equivalent to reducing σ_{tr}^2, σ_{st}^2, or increasing σ_{sr}^2. Only the ratio matters. We ran 10^4 trials. In each trial, h_{sr}, h_{st}, and h_{tr} are randomly generated as complex Gaussian variates, and the BER is averaged over the 10^4 trials.

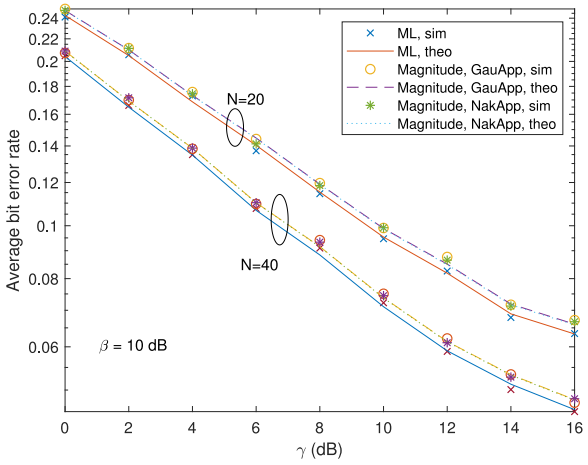

Fig. 2. ML and magnitude detectors for coherent detection with the Gaussian ambient signals when $N = 20, 40$.

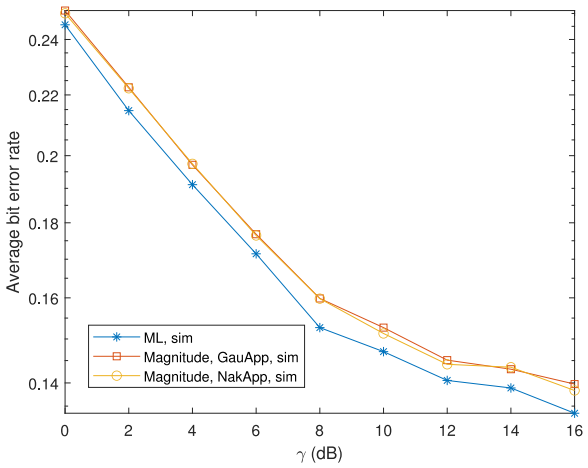

Fig. 3. ML and magnitude detectors for coherent detection with the Gaussian ambient signals when $\beta = 0$ dB and $N = 20$.

Figs. 2 and 3 show the case when coherent detection is performed for the Gaussian ambient signals, as derived in Section III-A. In these figures, "ML" refers to the detector in [18, eq. (8)] with theoretical BER in [18, eq. (13)] and [18, eq. (15)] as benchmark, "Magnitude, GauApp" refers to the new IED in (7) with theoretical approximate BER in (9) and (10) when $p = 1$, "Magnitude, NakApp" refers to the approximate magnitude detector in (14) with theoretical approximate BER in (16) and (17). The energy detector is not shown, as it is equivalent to the ML detector. First, one sees that the BER reduces when N increases, as expected. Second, the ML detector is slightly better than the magnitude

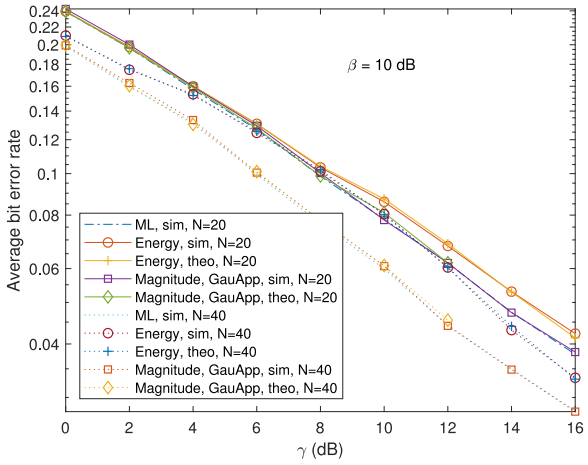

Fig. 4. ML, energy and magnitude detectors for coherent detection with PSK ambient signals when $N = 20, 40$.

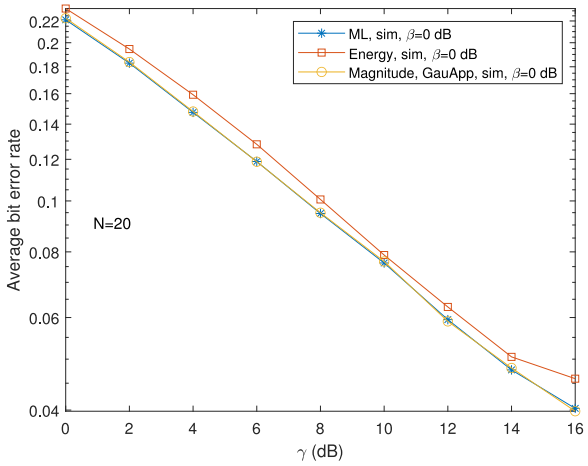

Fig. 5. ML, energy and magnitude detectors for coherent detection with PSK ambient signals when $\beta = 0$ dB and $N = 20$.

detectors, while the magnitude detector using the Gaussian approximation is almost identical to that using the Nakagami-m approximation. Finally, from Fig. 2, the theoretical BER agrees well with the simulated values. This shows that the Gaussian and Nakagami-m approximations are accurate in this case.

Figs. 4 and 5 show the case when coherent detection is performed for PSK ambient signals, as derived in Section III-B. In this case, ML refers to the detector in (21), "Energy" refers to the detector in (33) with theoretical BER in (35) and (36), Magnitude, GauApp refers to the detector in (26) with theoretical approximate BER in (28) and (29) when $p = 1$. Again, the BER performance improves when N increases. However, the improvement is not as large as that in Figs. 2 and 3. Comparing different detectors, one also sees that the magnitude detector has almost the same performance as the ML detector, both of which outperform the energy detector. Their performance gap increases when N increases. Finally, from Fig. 4, the theoretical results match well with the simulation results, showing the accuracy of the approximations in (28) and (29).

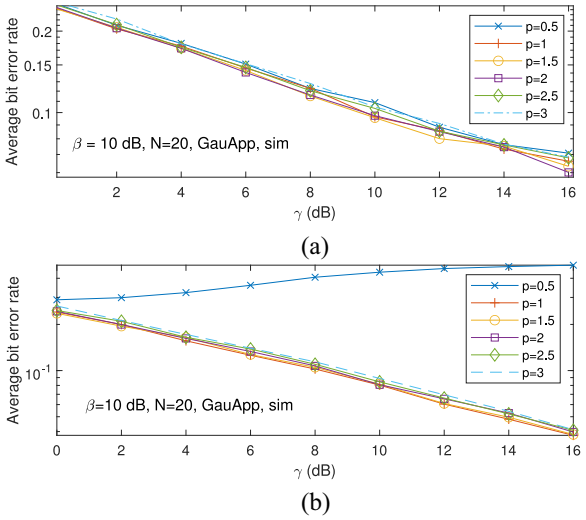

Fig. 6. Comparison of IED for coherent detection with the (a) Gaussian and (b) PSK ambient signals.

Fig. 6 compares the IED for coherent detection with the Gaussian and PSK ambient signals at different p. The case when $p = 1$ corresponds to the magnitude of the received signal. The case when $p = 2$ corresponds to the energy of the received signal. Other values of p correspond to different nonlinear distortion of the received signal. From part (a) of Fig. 6, one sees that the performance of IED first improves when p increases from 0.5 to 2 and then degrades when p increases further from 2 to 3. This confirms that the energy detector is optimum for Gaussian signals. Also, from part (b) of Fig. 6, the performance of IED monotonically degrades as p increases from 1 to 3, while $p = 0.5$ gives the worst performance where the BER increases with γ. This confirms that the magnitude detector has the best performance for PSK ambient signals. Comparing part (a) with part (b), one notices that the IED behaves differently for different assumptions of ambient signals and that the IED assuming PSK ambient signals is slightly better than that assuming the Gaussian signals. Note that the value of p could be negative but this is not considered here for two reasons. First, the calculation of negative order is complicated in hardware implementation. For low-cost low-power IoT applications, this may not be desirable. Second, the samples $|y[n]|$ could be close to zero due to the noise, in which case the detector may not be stable.

Figs. 7 and 8 show the case when partial coherent detection is performed for the Gaussian ambient signals, as derived in Section III-C. In these figures, "Energy, GauApp" and "Magnitude, GauApp" refer to the detector in (46) when $p = 2$ and $p = 1$, respectively. Since the ML detector has much higher complexity, it is not shown. Comparing the detectors, one sees that the energy detector outperforms the magnitude detector in all the conditions considered in this case, and the performance gain increases with N. Also, in Fig. 8, the BER increases when γ increases from 14 to 16 dB. This is probably caused by the Gaussian approximation and the approximation used in (40d), whose errors increase when β is small.

Figs. 9 and 10 show the case when partial coherent detection is performed for PSK ambient signals, as derived

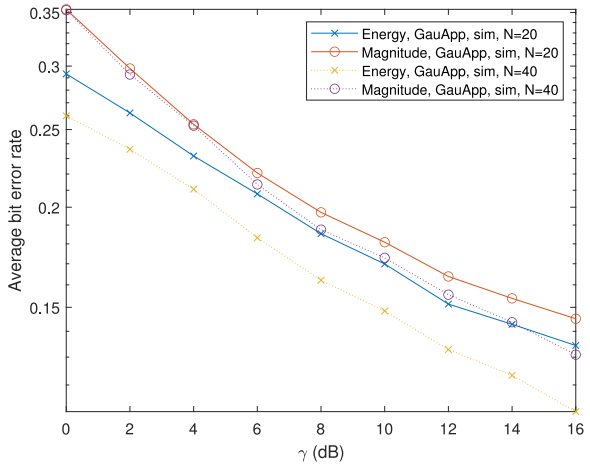

Fig. 7. Energy and magnitude detectors for partial coherent detection with the Gaussian ambient signals when $N = 20, 40$.

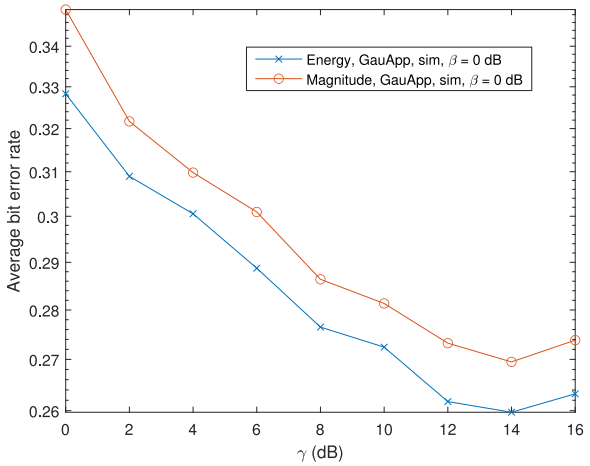

Fig. 8. Energy and magnitude detectors for partial coherent detection with the Gaussian ambient signals when $\beta = 0$ dB.

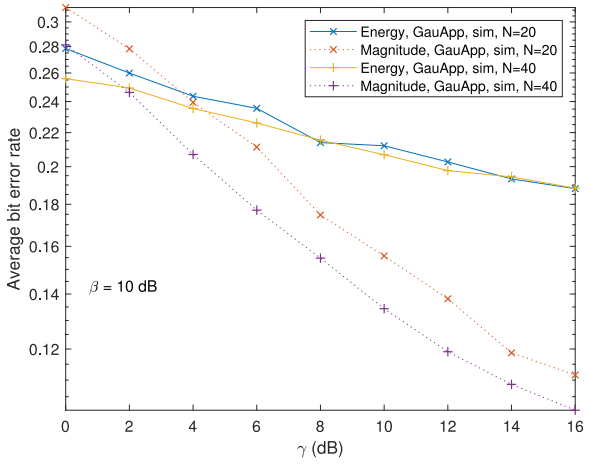

Fig. 9. Energy and magnitude detectors for partial coherent detection with PSK ambient signals when $N = 20, 40$.

in Section III-D. In these figures, Energy, GauApp and Magnitude, GauApp refer to the detector in (50) when $p = 2$ and $p = 1$, respectively. The ML detector has much higher complexity and therefore, is not shown. Similar to all the other

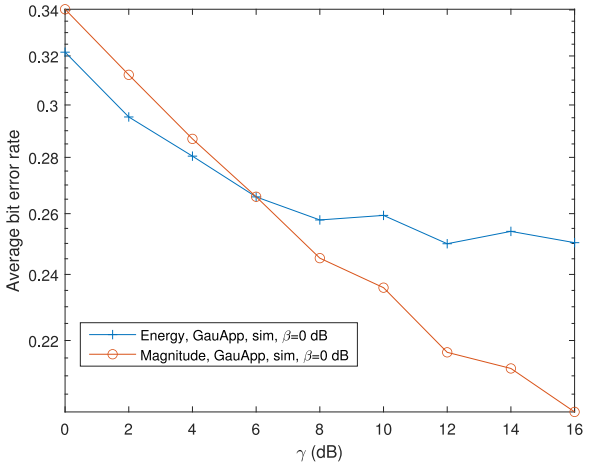

Fig. 10. Energy and magnitude detectors for partial coherent detection with PSK ambient signals when $\beta = 0$ dB.

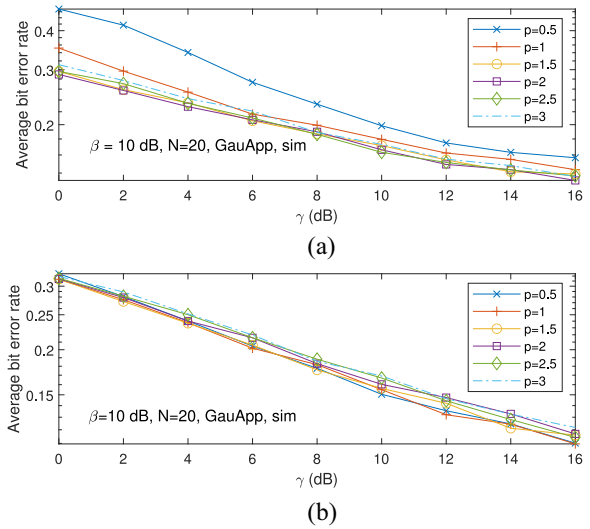

Fig. 11. Comparison of IED for partially coherent detection with the (a) Gaussian and (b) PSK ambient signals.

three cases, the BER performance improves when N increases. Comparing the two detectors, one sees that the energy detector is better when the SNR is small, while the magnitude detector is better when the SNR is large.

Fig. 11 compares the IED for partially coherent detection with the Gaussian and PSK ambient signals at different values of p. From part (a) of Fig. 11, the BER of the IED for Gaussian signals improves when p increases from 0.5 to 2 and then degrades when p further increases from 2 to 3, implying that the energy detector is the best option for Gaussian signals. From part (b) of Fig. 11, for small SNRs, all the IEDs with p smaller or equal to 2 have similar performances, while for large SNRs, the smaller p is, the better the BER performance will be. The magnitude detector has the best overall performance among all values of p examined for PSK ambient signals. These observations agree with those for coherent detectors and confirm that the energy detector is the best in the presence of the Gaussian source, while the magnitude detector is the best in the presence of the PSK ambient

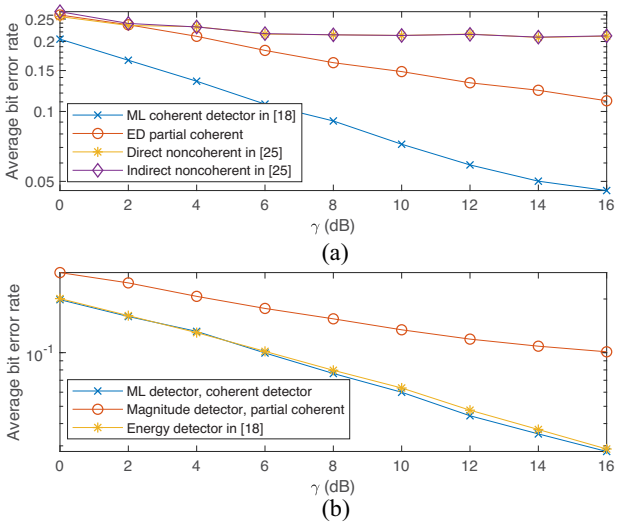

Fig. 12. Comparison of proposed detectors with existing detectors when $\beta = 10$ dB and $N = 40$. (a) Gaussian signals. (b) PSK signals.

source, for both coherent and partially coherent detection. Thus, in practice, $p = 1$ should be chosen for PSK ambient signals and $p = 2$ should be chosen for Gaussian ambient signals.

Fig. 12 compares the proposed detectors with existing detectors. In particular, for Gaussian ambient signals, the ML detector for coherent detection in [18, eq. (8)], the proposed ED detector for partial coherent detection in (46) with $p = 2$, and the existing noncoherent detectors using direct and indirect approaches in [25] are compared. One sees that the ML detector performs the best, followed by the ED detector in (46) and the noncoherent detectors in [25]. This is expected, as more channel knowledge often leads to better detection. For PSK signals, the proposed ML detector for coherent detection in (21), the proposed magnitude detector for partial coherent detection in (26) with $p = 1$, and the existing energy detector for coherent detection in [18] are compared. Again, the ML detector performs the best, followed by the energy detector and the magnitude detector. Also, in this case, channel knowledge is more important than detector design, as the two coherent detectors with full knowledge of h_0 and h_1 have similar performance, while the partial coherent magnitude detector with knowledge of only h_0 is the worst.

V. Conclusion

Four different cases of AmBC have been studied, assuming full and partial channel knowledge for Gaussian and PSK ambient signals, respectively. For the coherent detection with Gaussian and PSK ambient signals, the exact ML and ED detectors have been obtained, while moment-matching and Gaussian approximations have been used to derive the IED and MD detectors. For the partial coherent detection with Gaussian and PSK ambient signals, the ML detectors do not have closed-form expressions and are of similar complexity to those in [25], while the IED, ED, and MD detectors have been obtained using moment-matching and Gaussian approximations again in closed-form. The performances of these detectors have been analyzed and compared. Numerical results have shown that, for the coherent detection with Gaussian ambient signals, the ML and ED detectors are the best and equivalent to each other, while the MD detector is slightly worse and the IED detector is optimum when $p = 2$ as the ED detector. For the coherent detection with PSK ambient signals, the ML and MD detectors are the best, while the ED detector considerably under-performs them and the IED detector is optimum when $p = 1$ as the MD detector. For the partial coherent detection with Gaussian ambient signals, the ED detector outperforms the MD detector, and the IED detector is optimum when $p = 2$ as the ED detector. For the partial coherent detection with PSK ambient signals, the MD detector is overall better than the ED detector, while the IED detector is better for smaller p. The IED detector is very flexible, as it includes the best detectors in most cases as a special case. Numerical results have also shown that the coherent detection is always better than the corresponding partial coherent detection and that detectors for PSK ambient signals are slightly better than those for Gaussian ambient signals, under the same conditions. Future works include the extension of these detectors to frequency-selective channels, multiple tags, multiple antennas, and M-ary modulation schemes.

References

[1] C. Boyer and S. Roy, "Backscatter communication and RFID: Coding, energy, and MIMO analysis," *IEEE Trans. Commun.*, vol. 62, no. 3, pp. 770–785, Mar. 2014.

[2] V. Liu, A. Parks, V. Talla, S. Gollakota, D. Wetherall, and J. R. Smith, "Ambient backscatter: Wireless communication out of thin air," in *Proc. ACM SIGCOMM Conf.*, Hong Kong, Aug. 2013, pp. 39–50.

[3] J. Zhao, W. Gong, and J. Liu, "Spatial stream backscatter using commodity WiFi," in *Proc. 16th Annu. Int. Conf. Mobile Syst., Appl., Services*, 2018, pp. 191–203.

[4] D. Bharadia, K. Joshi, M. Kotaru, and S. Katti, "BackFi: High throughput WiFi backscatter,"' in *Proc. ACM SIGCOMM Conf. Special Interest Group Data Commun.*, London, U.K., 2015, pp. 283–296.

[5] S. -N. Daskalakis, J. Kimionis, A. Collado, M. M. Tentzeris, and A. Georgiadis, "'Ambient FM backscattering for smart agricultural monitoring," in *Proc. IEEE MTT-S Int. Microw. Symp.*, 2017, pp. 1339–1341.

[6] B. Kellogg, A. Parks, S. Gollakota, J. R. Smith, and D. Wetherall, "Wi-Fi backscatter: Internet connectivity for RF-powered devices," in *Proc. ACM SIGCOMM Conf.*, Chicago, IL, USA, Aug. 201, pp. 607–618.

[7] A. N. Parks, A. Liu, S. Gollakota, and J. R. Smith, "Turbocharging ambient backscatter communication," in *Proc. ACM SIGCOMM Conf.*, Chicago, IL, USA, Aug. 2014, pp. 619–630.

[8] B. Kellogg, V. Talla, S. Gollakota, and J. R. Smith, "Passive Wi-Fi: Bringing low power to Wi-Fi transmissions," in *Proc. ACM SIGCOMM*, Chicago, IL, USA, Aug. 2014, pp. 607–618.

[9] C. Yang, J. Gummeson, and A. Sample, "Riding the airways: Ultra-wideband ambient backscatter via commercial broadcast systems," in *Proc. IEEE Conf. Comput. Commun. (INFOCOM)*, Atlanta, GA, USA, May 2017, pp. 1–9.

[10] T. Hara, R. Takahashi, and K. Ishibashi, "Ambient OFDM pilot-aided backscatter communications: Concept and design," *IEEE Access*, vol. 9, pp. 89210–89221, 2021.

[11] D. Darsena, G. Gelli, and F. Verde, "Modeling and performance analysis of wireless networks with ambient backscatter devices," *IEEE Trans. Communi.*, vol. 65, no. 4, pp. 1797–1814, Apr. 2017.

[12] D. Darsena, G. Gelli, and F. Verde, "Cloud-aided cognitive ambient backscatter wireless sensor networks," *IEEE Access*, vol. 7, pp. 57399–57414, 2019.

[13] J. Chen, H. Yu, Q. Guan, G. Yang, and Y.-C. Liang, "Spatial modulation based multiple access for ambient backscatter networks," *IEEE Commun. Lett.*, vol. 26, no. 1, pp. 197–201, Jan. 2022.

[14] N. V. Huynh, D. T. Hoang, X. Lu, D. Niyato, P. Wang, and D. I. Kim, "Ambient backscatter communications: A contemporary survey," *IEEE Commun. Surveys Tuts.*, vol. 20, no. 4, pp. 2889–2922, 4th Quart., 2018.

[15] G. Wang, F. Gao, Z. Dou, and C. Tellambura, "Uplink detection and BER analysis for ambient backscatter communication systems," in *Proc. IEEE Global Commun. Conf. (GLOBECOM)*, San Diego, CA, USA, Dec. 2015, pp. 1–6.
[16] K. Lu, G. Wang, F. Qu, and Z. Zhong, "Signal detection and BER analysis for RF-powered devices utilizing ambient backscatter," in *Proc. Int. Conf. Wireless Commun. Signal Process. (WCSP)*, Nanjing, China, Oct. 2015, pp. 1–5.
[17] G. Wang, F. Gao, R. Fan, and C. Tellambura, "Ambient backscatter communication systems: Detection and performance analysis," *IEEE Trans. Commun.*, vol. 64, no. 11, pp. 4836–4846, Nov. 2016.
[18] J. Qian, F. Gao, G. Wang, S. Jin, and H. Zhu, "Semi-coherent detection and performance analysis for ambient backscatter system," *IEEE Trans. Commun.*, vol. 65, no. 12, pp. 5266–5279, Dec. 2017.
[19] J. Qian, F. Gao, G. Wang, S. Jin, and H. Zhu, "Semi-coherent detector of ambient backscatter communication for the Internet of Things," in *Proc. IEEE SPAWC*, Sapporo, Japan, Jul. 2017, pp. 1–5.
[20] Q. Tao, C. Zhong, H. Lin, and Z. Zhang, "Symbol detection of ambient backscatter systems with Manchester coding," *IEEE Trans. Wireless Commun.*, vol. 17, no. 6, pp. 4028–4038, Jun. 2018.
[21] J. Qian, F. Gao, G. Wang, S. Jin, and H. Zhu, "Noncoherent detections for ambient backscatter system," *IEEE Trans. Wireless Commun.*, vol. 16, no. 3, pp. 1412–1422, Mar. 2017.
[22] Y. Liu, G. Wang, Z. Dou, and Z. Zhong, "Coding and detection schemes for ambient backscatter communication systems," *IEEE Access*, vol. 5, pp. 4947–4953, 2017.
[23] Q. Zhang, H. Guo, Y.-C. Liang, and X. Yuan, "Constellation learning-based signal detection for ambient backscatter communication systems," *IEEE J. Sel. Areas Commun.*, vol. 37, no. 2, pp. 452–463, Feb. 2019.
[24] T. Zeng, G. Wang, Y. Wang, Z. Zhong, and C. Tellambura, "Statistical covariance based signal detection for ambient backscatter communication systems," in *Proc. IEEE 84th Veh. Technol. Conf. (VTC-Fall)*, Montreal, QC, Canada, Sep. 2016, pp. 1–5.
[25] S. Guruacharya, X. Lu, and E. Hossain, "Optimal non-coherent detector for ambient backscatter communication system," *IEEE Trans. Veh. Technol.*, vol. 69, no. 12, pp. 16197–16201, Dec. 2020.
[26] J. K. Devineni and H. S. Dhillon, "Non-coherent signal detection and bit error rate for an ambient backscatter link in time-selective link," *IEEE Trans. Commun.*, vol. 69, no. 1, pp. 602–618, Jan. 2021.
[27] J. K. Devineni and H. S. Dhillon, "Non-coherent detection and bit error rate for an ambient backscatter link under fast fading," in *Proc. IEEE Globecom*, Waikoloa, HI, USA, Dec. 2019, pp. 1–6.
[28] J. K. Devineni and H. S. Dhillon, "Multi-antenna non-coherent detection of ambient backscatter under time-selective fading," in *Proc. IEEE Globecom*, Taibei, Taiwan, Dec. 2020, pp. 1–6.
[29] J. K. Devineni and H. S. Dhillon, "Manchester encoding for non-coherent detection of ambient backscatter in time-selective fading," *IEEE Trans. Veh. Technol.*, vol. 70, no. 5, pp. 5109–5114, May 2021.
[30] G. Yang, Z. Luo, N. Jin, Y.-C. Liang, Y. Xu, and G. Wang, "Non-coherent parallel detection of ambient backscatter communications with multiple tags," *IEEE Trans. Veh. Technol.*, vol. 72, no. 4, pp. 5344–5349, Apr. 2023.
[31] J. Qian, A. N. Parks, J. R. Smith, F. Gao, and S. Jin, "IoT communications with M -PSK modulated ambient backscatter: Algorithm, analysis, and implementation," *IEEE Internet Things J.*, vol. 6, no. 1, pp. 844–855, Feb. 2019.
[32] R. Duan, R. Jantti, M. ElMossallamy, Z. Han, and M. Pan, "Multi-antenna receiver for ambient backscatter communication systems," in *Proc. IEEE SPAWC*, Kalamata, Greece, Jun. 2018, pp. 1–5.
[33] W. Zhao, G. Wang, R. Fan, L.-S. Fan, and S. Atapattu, "Ambient backscatter communication systems: Capacity and outage performance analysis," *IEEE Access*, vol. 6, pp. 22695–22704, 2018.
[34] J. K. Devineni and H. S. Dhillon, "Ambient backscatter systems: Exact average bit error rate under fading channels," *IEEE Trans. Green Commun. Netw.*, vol. 3, no. 1, pp. 11–25, Mar. 2019, doi: 10.1109/TGCN.2018.2880985.
[35] G. Yang, Y.-C. Liang, R. Zhang, and Y. Pei, "Modulation in the air: Backscatter communication over ambient OFDM carrier," *IEEE Trans. Commun.*, vol. 66, no. 3, pp. 1219–1233, Mar. 2018.
[36] D. Darsena, "Noncoherent detection for ambient backscatter communications over OFDM signals," *IEEE Access*, vol. 7, pp. 159415–159425, 2019.
[37] M.A. ElMossallamy, M. Pan, R. Jäntti, K. G. Seddik, G. Li, and Z. Han, "Noncoherent backscatter communications over ambient OFDM signals," *IEEE Trans. Commun.*, vol. 67, no. 5, pp. 3597–3611, May 2019.
[38] C.-H. Kang, W.-S. Lee, Y.-H. You, and H.-K. Song, "Signal detection scheme in ambient backscatter system with multiple antennas," *IEEE Access*, vol. 5, pp. 14543–14547, 2017.
[39] Q. Tao, C. Zhong, X. Chen, H. Lin, and Z. Zhang, "Maximum-eigenvalue detector for multiple antenna ambient backscatter communication systems," *IEEE Trans. Veh. Technol.*, vol. 68, no. 12, pp. 12411–12415, Dec. 2019.
[40] W. Liu, S. Shen, D. H. K. Tsang, and R. Murch, "Enhancing ambient backscatter communication utilizing coherent and non-coherent space-time codes," *IEEE Trans. Wireless Commun.*, vol. 20, no. 10, pp. 6884–6897, Oct. 2021.
[41] C. Chen, G. Wang, H. Guan, Y.-C. Liang, and C. Tellambura, "Transceiver design and signal detection in backscatter communication systems with multiple-antenna tags," *IEEE Trans. Wireless Commun.*, vol. 19, no. 5, pp. 3273–3288, May 2020.
[42] Q. Tao, C. Zhong, X. Chen, H. Lin, and Z. Zhang, "Optimal detection for ambient backscatter communication systems with multiantenna reader under complex Gaussian illuminator," *IEEE Internet Things J.*, vol. 7, no. 12, pp. 11371–11383, Dec. 2020.
[43] G. Yang, Q. Zhang, and Y.-C. Liang, "Cooperative ambient backscatter communications for green Internet-of-Things," *IEEE Internet Things J.*, vol. 5, no. 2, pp. 1116–1130, Apr. 2018.
[44] Y. Chen, "Improved energy detector for random signals in Gaussian noise," *IEEE Trans. Wireless Commun.*, vol. 9, no. 2, pp. 558–563, Feb. 2010.
[45] N. Amin, N. W. Jye, and M. Othman, "A BPSK backscatter modulator design for RFID passive tags," in *Proc. IEEE Int. Workshop Radio-Freq. Integr. Technol.*, Singapore, Dec. 2007, pp. 262–265.
[46] C. Zhang, G. Wang, P. D. Diamantoulakis, F. Gao, and G. K. Karagiannidis, "Interference-free transceiver design and signal detection for ambient backscatter communication systems over frequency-selective channels," 2018, *arXiv:1812.11278*.
[47] J. G. Proakis, *Digital Communications*, 4th ed. New York, NY, USA: McGraw-Hill, 2001.
[48] I. S. Gradshteyn and I. M. Ryzhik, *Tables of Integrals, Series and Products*, 6th ed. London, U.K.: Academic, 2000.
[49] H. H. Zeng and L. Tong, "Blind channel estimation using the second-order statistics: Algorithms," *IEEE Trans. Signal Process.*, vol. 45, no. 8, pp. 1919–1930, Aug. 1997.
[50] Y. Chen and N. C. Beaulieu, "NDA estimation of SINR for QAM signals," *IEEE Commun. Lett.*, vol. 9, no. 8, pp. 688–690, Aug. 2005.

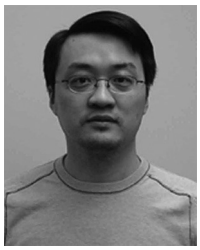

Yunfei Chen (Senior Member, IEEE) received the B.E. and M.E. degrees in electronics engineering from Shanghai Jiaotong University, Shanghai, China, in 1998 and 2001, respectively, and the Ph.D. degree from the University of Alberta, Edmonton, AB, Canada, in 2006.

He is currently working as a Professor with the Department of Engineering, Durham University, Durham, U.K. His research interests include wireless communications, performance analysis, joint radar communications designs, cognitive radios, wireless relaying, and energy harvesting.

Wei Feng (Senior Member, IEEE) received the B.S. and Ph.D. degrees from the Department of Electronic Engineering, Tsinghua University, Beijing, China, in 2005 and 2010, respectively.

He is currently a Professor with the Department of Electronic Engineering, Tsinghua University. His research interests include maritime communication networks, large-scale distributed antenna systems, and coordinated satellite–UAV–terrestrial networks.

Dr. Feng serves as an Assistant to the Editor-in-Chief for *China Communications* and an Editor for IEEE TRANSACTIONS ON COGNITIVE COMMUNICATIONS AND NETWORKING.